Chinese Journal of Structural Chemistry

ARTICLE

Atomically Thin 2D TiO_2 Nanosheets with Ligand Modified Surface for Ultra-sensitive Humidity Sensor

Jianze Xiao[1,2], Zhihua Fu[2], Guane Wang[2,3], Xiaoliang Ye[2]* and Gang Xu[2,3,4]*

[1]*College of Chemistry, Fuzhou University, Fuzhou 350116, China*

[2]*State Key Laboratory of Structure Chemistry, Fujian Institute of Research on the Structure of Matter, Chinese Academy of Science, Fuzhou 350002, China*

[3]*University of Chinese Academy of Sciences, Beijing 100049, China*

[4]*Fujian Science & Technology Innovation Laboratory for Optoelectronic Information of China, Fuzhou 350108, China*

ABSTRACT As a kind of two-dimensional (2D) nanostructured materials, metal oxide nanosheets (MONS) are attractive and promising humidity sensing materials due to their considerable surface area, good charge carrier transportation, and designable surface functional groups properties. Nevertheless, the ultra-thin MONS modified with active functional groups for humidity sensing are still rare. As a proof of concept, the atomically thin TiO_2 nanosheets with high surface area and electron-donating amino groups are prepared by a structure-maintained post-ligand modification strategy. The fabricated TiO_2-based sensors demonstrate superior humidity sensing performance with high response, short response time, narrow hysteresis, and ultra-low theoretical limit of detection of about 15 ppm. Additionally, the possible mechanism is proposed from the AC complex impedance measurements and DC instantaneous reverse polarity experiments. This work provides a possible path for developing the high-performance 2D nanostructured metal oxides-based humidity materials through the surface chemical method.

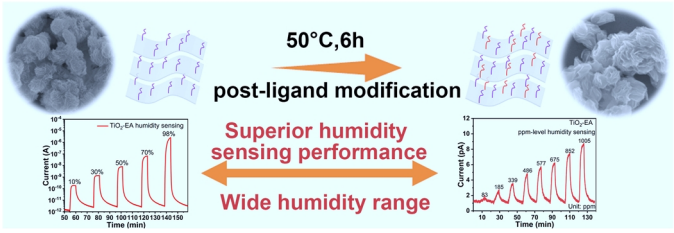

Keywords: TiO_2 nanosheet, ligand modification, ultra-sensitive, chemiresistive, humidity sensing

n INTRODUCTION

Humidity is an important physical parameter that affects people's daily life and production, especially in environment monitoring, agricultural production, industrial manufacture, food storage, and medical diagnosis.[1-5] Since the rapid development of the Internet of Things (IoT) and artificial intelligence (AI), the humidity monitoring devices with convenient fabrication, extraordinary sensitivity, fast response and recovery, low power consumption, and low-cost materials are eagerly required.[6] Generally, a superior humidity sensing material should meet several essential rules: 1) high specific surface area, to better perceive the minimal variation of ambient humidity since the contacts between H_2O molecules and sensing layer take place first on the surface, 2) abundant active sites on the surface, to instantly interact with physical absorbed H_2O molecules for faster response speed and higher sensitivity.[7,8] Based on these requirements, the two-dimensional (2D) nanostructured materials with advantages of the high area to volume ratio, fully exposed active sites, and facile surface functionalization have been considered as a promising material for humidity sensing, which also provides an ideal platform to study the sensing process between the sensitive layers and water molecules.[9-11]

The chemical and physical properties of 2D nanostructured materials could be significantly improved by the reasonable design of surface-coordinated chemical environments.[12-19] Surface chemistry such as surface functionalization and chemical modification, which could distinctly tune the conductivity, improve the charge carriers or mass transfer, or enhance the interaction between substrates and targeted molecules, could efficiently improve the sensing performance of 2D nanostructured materials.[20-25] However, the structural variation of those 2D materials usually occurs during the vigorously chemical modification, which obstructs the construction of the structure-activity relationship.[26-28] Therefore, a strategy for structure-maintained post-modification with a slight adjustment in surface coordination environment is urgently desired. Among 2D nanostructured materials, ultra-thin metal oxide nanosheets (MONS) have demonstrated much better charger carrier transportation and gas detection sensitivity.[29-31] With the principle of surface modification by introducing appropriate functional groups, ultra-thin MONS would provide ultra-high humidity sensing performance. Unfortunately, MONS-based humidity sensing materials are still in their infancy.[32-37] There is still much room for developing ultra-sensitive sensing materials to serve as the ultra-low humidity environment monitor.

Herein, 2D ultra-thin TiO_2 nanosheets with various functional groups modification were successfully prepared via a facile strategy of structure-maintained post-ligand modification (Figure 1a). As-prepared 3 cases of TiO_2 nanosheets were utilized to demonstrate the effect of diverse surface chemical environments for chemiresistive humidity sensing. The sensor shows excellent performance with a noticeable conductivity enhancement of more than 10^6 from dry air to 98% of relative humidity (RH), as well as the shortest response time of 98.4 s. Particularly, the ultra-thin TiO_2 nanosheet sensor devices coordinated with ethylene glycol (EG) and ethylenediamine (EA) exhibit outstanding sensing per-

DOI: 10.14102/j.cnki.0254-5861.2022-0046

formance toward ppm-level humidity with the ultra-low theoretical limit of detection of about 15 ppm. Additionally, the possible mechanism was proposed to explain the excellent humidity sensing behavior after the AC complex impedance measurements and DC instantaneous reverse polarity experiments. The surface property of the 2D ultra-thin TiO_2 nanosheet played a vital role in the ultra-low humidity sensing process, in which the electron-donating amino groups of TiO_2-EA are more beneficial than the electron-withdrawing carboxylate radical of TiO_2-OA for the free migration of electrons in ultra-low humidity sensing process.

n RESULTS AND DISCUSSION

The EG coordinated TiO_2 nanosheets (TiO_2-EG) with a BET surface area of ~320 $m^2 \cdot g^{-1}$ (Figure S5) were synthesized via a modified solvothermal method (see details in Supporting information, Figure 1a). The powder X-ray diffraction (PXRD) pattern (Figure 1b) illustrates that these TiO_2-EG powders are a metastable polymorph of TiO_2(B) which owns a less symmetrical monoclinic structure and belongs to the C2/m space group (card JCPDS No. 46-1238).[38,39] The surfaces modified with ethylenediamine (EA) and oxalate (OA) on TiO_2 nanosheets were prepared by a facile post-ligand modification strategy (Figure 1a), and were labeled as TiO_2-EA and TiO_2-OA, respectively. The PXRD patterns of TiO_2-EA and TiO_2-OA (Figure 1b) are similar with that of TiO_2-EG, implying that the structure of TiO_2-EG is still maintained after post-ligand modification. Furthermore, the broad PXRD peaks of three samples indicate significantly decreased thickness of TiO_2 nanosheets with only a few layers, which could be verified by the atomic force microscopy (AFM) analysis in the following test.[40,41]

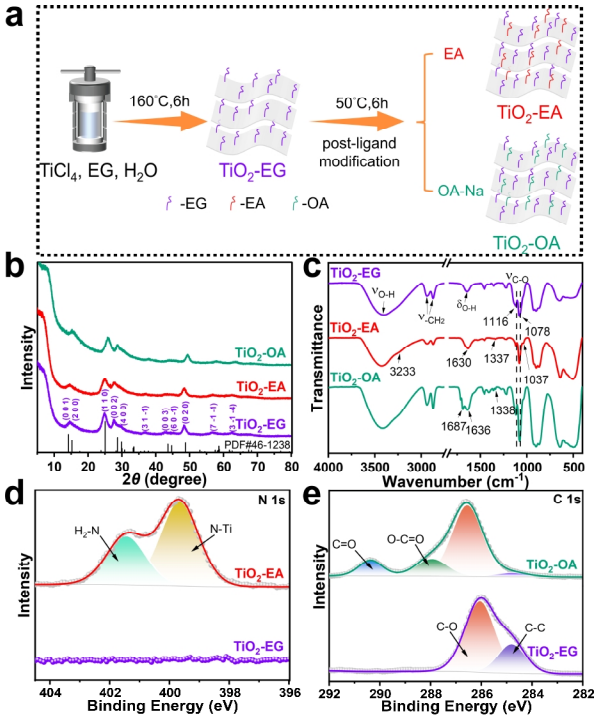

Figure 1. (a) The illustration of synthesis and post-modification process (b) PXRD patterns and (c) FT-IR spectra of TiO_2-EG, TiO_2-EA, and TiO_2-OA powders. XPS spectra of (d) N 1s and (d) C 1s.

The surface chemical environments of the three TiO_2 samples were determined by Fourier transform infrared spectroscopy (FT-IR) and X-ray photoelectron spectroscopy (XPS). As shown in Figure 1c, compared to that of TiO_2-EG and ethylenediamine (Figure S6a), the FT-IR spectra of TiO_2-EA show additional adsorption bands at 3233 and 1630 cm^{-1}, which are assigned to stretching and bending vibrations of -NH_2 groups, respectively.[42] The adsorption bands at 1337 and 1037 cm^{-1} for C–N vibrations further confirm the presence of the amine-containing groups on the surface of TiO_2-EA nanosheets. Similarly, compared with the IR spectra of sodium oxalate (Figure S6b), the adsorption bands located at 1636 and 1338 cm^{-1} are assigned to the asymmetric and symmetric stretching vibrations of COO^-, respectively, indicating the presence of COO^- on the surface of TiO_2-OA nanosheets.[43] Additionally, the obviously sharped and increased adsorption band intensity at about 1078 and 1116 cm^{-1} further evidences the increased amount of -C–O. Meanwhile, XPS characterization was also performed to verify the coordination of EA and OA groups on TiO_2 nanosheets. Different from that of TiO_2-EG, the N 1s spectrum of TiO_2-EA (Figure 1d) exhibits two major signals located at 401.5 and 399.7 eV, which are assigned to the free -NH_2 and -N-H coordinated with the Ti center, respectively.[44] The new raising signals of the C 1s spectrum located at 287.9 and 290.4 eV (Figure 1e) are ascribed to the O–C=O and C=O groups of COO^- on TiO_2 surface, respectively, confirming the successful modification of the OA group.[43] These results also could be verified by the O 1s spectra of TiO_2-EG, TiO_2-EA, and TiO_2-OA (Figure S6c).

Scanning electron microscope (SEM) measurements of TiO_2-EG, TiO_2-EA, and TiO_2-OA powders depict similar plicated nanosheet morphology, because of the tension of ultra-thin geometry (Figure 2a–2c and Figure S7g–7i). From transmission electron microscopy (TEM) images (Figure 2d–2f), the nanosheet morphology with large size of three TiO_2 remains after post-ligand modification. The STEM element mapping of TiO_2-EA also confirms the existence of surface N species (Figure S6d), further revealing the successful modification of EA on the surface of TiO_2 nanosheets. The thicknesses of TiO_2 samples checked by AFM are ranged from 1.4 to1.8 nm (Figure 2g–2i and Figure S7a–7f). With such a few nanometers thickness, charge transportation between 2D TiO_2 nanosheets and H_2O molecules would be accelerated in a shortened conduction path, which is a candidate as the high-performance humidity sensing material.

The humidity-sensing performances of the three kinds of TiO_2 sensors were evaluated by measuring their electrical current change under different RH conditions at ambient temperature. The parameters including humidity sensitivity, response time, recovery time, cycle stability, and hysteresis were evaluated. The real-time dynamic current response-recovery plots of TiO_2-EG, TiO_2-EA, and TiO_2-OA show that the prepared humidity sensors all demonstrate good response-recovery characteristics and significant step current response to a broad range of RH from 10 to 98%, as well as an excellent signal to noise ratio (Figure 3a and Figure S9a–9b). It can be found that the sensor's current increases rapidly when the RH is introduced from 10% to a higher RH level and then begins to recover to baseline current when the dry air is introduced back to the test chamber. When switching

DOI: 10.14102/j.cnki.0254-5861.2022-0046

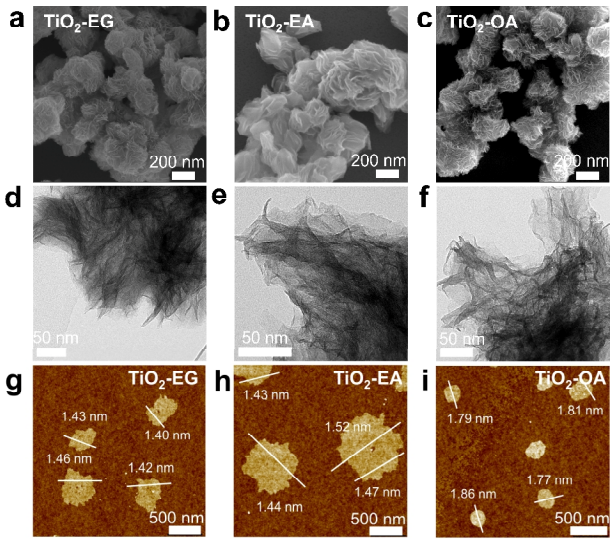

Figure 2. (a–c) SEM images, (d–f) TEM images, and (g–i) AFM images of TiO_2-EG, TiO_2-EA, and TiO_2-OA nanosheets.

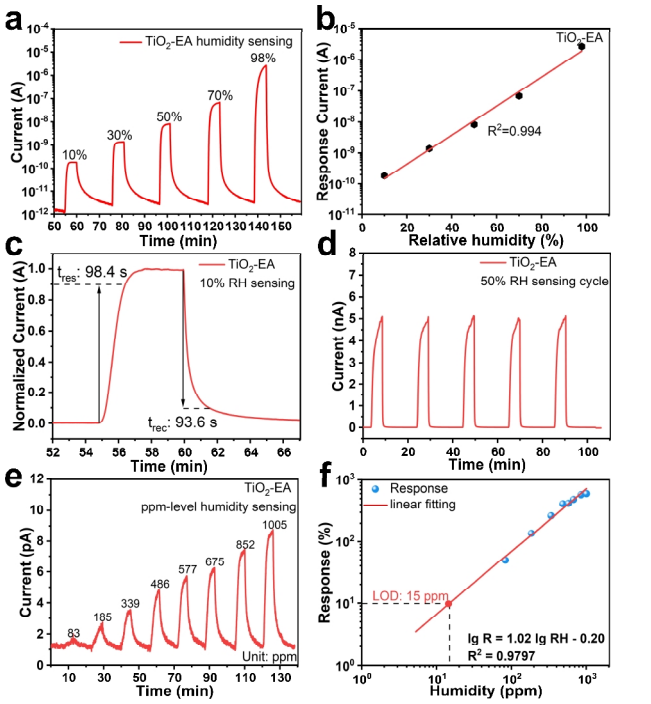

Figure 3. (a) The real-time dynamic current response-recovery plots of TiO_2-EA. (b) The response current plot of TiO_2-EA at different RH. (c) The response-10%RH sensing plots of TiO_2-EA. (d)The response-recovery cycle plots of TiO_2-EA at 50%RH. (e) The real-time ppm-level humidity sensing plot and (f) theoretical limit of detection calculation of TiO_2-EA.

from dry air to 98% RH, the currents of the TiO_2-EG, TiO_2-EA, and TiO_2-OA sensors all increase dramatically by about six orders of magnitude, indicating an excellent humidity sensitivity of 2D ultra-thin TiO_2 nanosheets-based sensor.

The response currents of the 2D ultra-thin TiO_2 nanosheets-based sensors at different RH were collected and plotted in Figure 3b and Figure S4. It can be seen that the sensor fabricated by TiO_2-EA nanosheets displays better linearity with the linearity fit correlation R^2 of 0.994 than that of TiO_2-EG and TiO_2-OA (Figure S10). For practical application of humidity sensors, good linear dependence relation of RH and response is especially important and is the evaluation criteria of accurate humidity detection.

The response-relative humidity sensing plots of TiO_2-EG, TiO_2-EA, and TiO_2-OA are shown in Figure 3c and Figure S9c–9d, while they are exposed to the 10%RH. Due to the atomically thin structure and abundant active functional groups on the surface, the response times of TiO_2-EG, TiO_2-EA, and TiO_2-OA samples are approximately 168.0, 98.4, and 124.1 s, respectively. These results suggest that the response-recovery dynamics of TiO_2-EA is faster than that of the other two sensors, which may originate from the rapid adsorption-response-desorption of water molecules on the surface of TiO_2-EA. In the cycling tests, the response-recovery plots of TiO_2-EA upon 50%RH with five consecutive test cycles (Figure 3d) display excellent stability, while the other two TiO_2 samples decay seriously (Figure S9e–9f). Besides, the TiO_2-EA has the narrowest hysteresis (Figure S11a) compared with TiO_2-EG and TiO_2-OA in the whole humidity range of 10–98% (Figure S11b–11c). These results indicate superior reliability and reversibility of humidity detection on TiO_2-EA.

Notably, it can be found that the TiO_2-EA based humidity sensors show the best sensing performance toward low relative humidity of 10% RH with a current increasing more than two orders of magnitude, compared with the other two TiO_2 samples, which demonstrates a fantastic potential of ppm-concentration humidity detection. However, rarely related chemiresistive humidity sensing literature has reported about the ppm-concentration humidity detection. To further investigate the potential of TiO_2-EA for ultra-low humidity sensing, we tested the ppm-concentration humidity sensing performance. The commercial dry N_2 is used as the purge gas for work baseline and carrier gas of the different ppm-concentration humidity. The concentration of ultra-low humidity was determined by the commercial dew point meter. Figure 3e shows the real-time ppm-level humidity sensing plot of TiO_2-EA and indicates that the TiO_2-EA sensor has good humidity sensitivity ranging from 83 ppm to 1005 ppm. The TiO_2-EA sensor has a response value of about 49.1% upon exposure to 83 ppm humidity and displays a theoretical limit of detection of 15 ppm (Figure 3f, calculated from the principle of 10% response method) with linearity fitting correlation R^2 = 0.980. Compared with other types of ultra-low humidity sensing materials reported in the literature, the prepared ultra-thin TiO_2 nanosheets have excellent humidity sensing performance in terms of humidity sensing range (15 ppm to 98% RH) and response-recovery time (98.4 and 93.6 s), which is comparable to the commercial capacitive-type γ-Al_2O_3 (Table S2). The excellent ppm-level humidity sensitivity could be related to the electron-donating property of the amino groups on the TiO_2-EA surface.

In order to further investigate the humidity sensing mechanism and distinguish the conduction processes at different RH of the 2D ultra-thin TiO_2-EA nanosheets-based sensor, typical AC complex impedance measurement of the TiO_2-EA nanosheets-based sensor was carried towards different RH in the frequency range

DOI: 10.14102/j.cnki.0254-5861.2022-0046

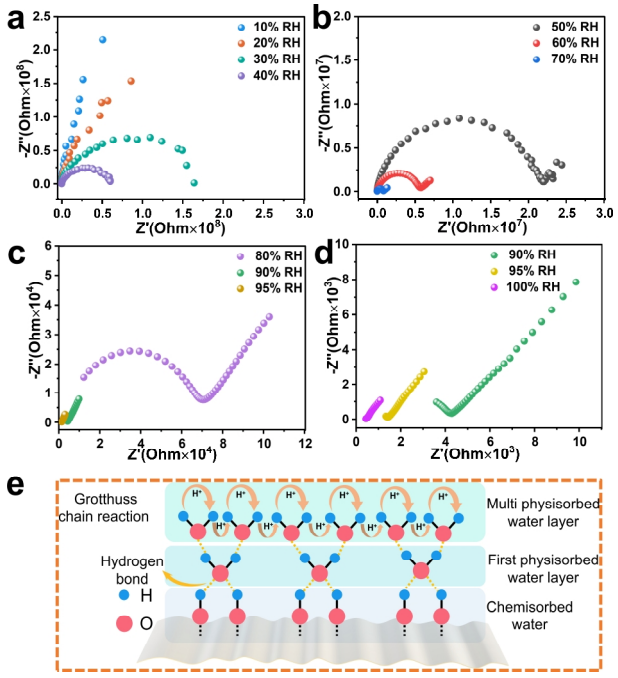

Figure 4. (a–d) The Nyquist plots of TiO_2-EA at different RH levels and (e) the schematic diagram of the humidity sensing mechanism of 2D nanostructured ultra-thin TiO_2-EA.

of 10^6–10 Hz. As shown in Figure 4a–4d, the Nyquist plots change from arc (low RH levels: 10–40%) to semicircle with a short linear tail (medium RH levels: 50–80%) and finally to the nearly linear line (high RH levels: 90–100%), which corresponds to the surface chemisorption and physisorption process of water molecules, respectively, and contains water-related polarization and conduction mechanism in humidity sensing process.

According to the sensing mechanism of metal oxides described in the reported literature, the electron depletion layer theory plays a crucial role in the gas sensing process, in which the electrons (e^-) on the surface of TiO_2-EA are easy to be trapped by the pre-adsorbed oxygen ($O_{2(ads.)}$) and then induce the generation of active oxygen species ($O_{2(ads.)}^-$) when the temperature is below 100 °C, as well as a high resistance value.[45] When the TiO_2-EA sensor is exposed to low RH levels (10–40%), only limited water molecules could be chemisorbed on the nanosheet surface, and the electrons are released back to the surface of TiO_2-EA. The chemisorbed water molecules dissociate into OH^- and H^+ groups, and then the H^+ and another adjacent surface O^{2-} will form the second OH^- group as equation 1.

$$H_2O + O^{2-} = 2OH^- \quad (1)$$

Therefore, the conduction at room temperature originates from the proton hopping transportation mechanism. The protons cross the barrier from one position to another on the 2D nanosheet surface acting as charge carriers. Hence, the impedance of the TiO_2-EA sensor decreases, but the coverage of water molecules and the concentration of protons on the sensing film surface are low, and the chemically adsorbed water molecules are not enough to form a continuous layer of water. As a result, the electrolytic conduction is very difficult and the impedance is still enormous. As shown in Figure 4a, the Nyquist plots exhibit an arc with a very large radius of curvature in a low humidity atmosphere (10–40%). According to the impedance plot, the conduction of the sensor can be modelled by a resistor R_1 connected in series with a parallel circuit of a resistor R_2 and a constant phase element (CPE_1) (Figure S12a). And it represents the charge transfer between the TiO_2-EA nanosheets and the chemisorbed adsorbed water molecules.

When the humidity is at a medium level of 50–80%, more and more water molecules are bound to the underlying chemisorbed water layer by physical adsorption, resulting in the formation of the first continuous water layer. In this case, the OH^- groups provide abundant nucleation sites for other water molecules to physically adsorb by hydrogen bonds. And the physically absorbed water molecules will dissociate under the electrostatic field of the chemisorbed OH^- group and form H_3O^+ ions. The amount of H_3O^+ ions also increases remarkably with the formation of multilayer water molecules. These H_3O^+ ions and protons can migrate freely in continuous water layers. In addition, according to the Grotthuss ion transfer theory, the H^+ can transfer to another adjacent water molecule through the Grotthuss chain mechanism as equation 2, which plays a key role in the conduction process of higher RH levels.[46]

$$H_3O^+ + H_2O \leftrightarrow H_3O^+ + H_2O \quad (2)$$

These ions can diffuse in the water molecule layers and serve as dominant charge carriers, resulting in a considerable decrease of grain boundary resistance of TiO_2-EA and interface resistance of sensing film/electrode. As shown in Figure 4b, the radius of the semicircle at high frequency sharply decreases, with a linear tail appearing at low frequency, which represents the Warburg impedance and it is a natural result from electrolytic conduction and the diffusion process of ions (H_3O^+ and H^+) at the sensing film/electrode interface. In this stage, the conduction of the sensor can be described by an equivalent circuit of parallel resistance (R_2)/constant phase element (CPE_1) and a Warburg resistance (W_1) (Figure S12b). The Warburg resistance (W_1) describes the ion diffusion of H_3O^+ and H^+ on the sensing film/electrode interface.

With the relative humidity raising to high RH levels of 90–100%, the coverage of water molecule layers on the sensing film surface is full enough. The physical adsorption of water molecules tends to saturate and forms liquid water layer, which is beneficial for the hydration of H_3O^+ to protons as the following equation 3.

$$H_3O^+ \leftrightarrow H_2O + H^+ \quad (3)$$

As a result, more H_3O^+ can dissociate and more H^+ will be generated on the sensing film surface. The diffusion of these ions between nanosheets becomes the dominant conduction mechanism. As shown in Figure 4c–4d, the semicircle radius of the impedance plot sharply decreases to a short arc with a linear tail connected. The equivalent circuit can be modelled by a combination circuit of parallel resistance (R_2)/constant phase element (CPE_1) and a Warburg resistance (W_1) (Figure S12c).

In order to verify the results of the AC impedance spectra measurements, DC instantaneous reverse polarity experiments are carried out to differentiate contributions from ions and electrons.[47] The operation principle is that when the humidity sensor reaches stability in the specific humidity environments, the conducting

DOI: 10.14102/j.cnki.0254-5861.2022-0046

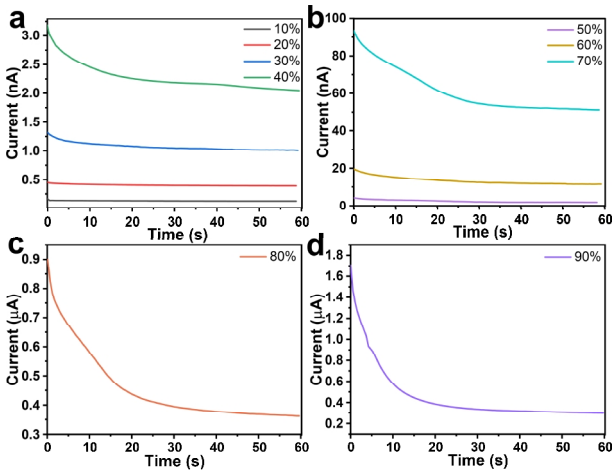

Figure 5. The curves of current vs. time of the TiO_2-EA based sensor at various RH obtained by the DC instantaneous reverse polarity experiments: (a) 10–40%; (b) 50–70%; (c) 80%; (d) 90%.

charge carrier will change with the direction of the electrical current because different charge carriers have different transmitting speeds. The corresponding DC experiment circuit is shown in Figure S8 with a bias voltage of 1 V and the results are shown in Figure 5.

The total current typically contains two parts: initial current and final current. When 1 V bias voltage is applied to TiO_2-EA sensing film, it can be polarized and the total current will decay exponentially and gradually turn to the final current value due to the different transfer rates of different conductive charge carriers. These different stages suggest different conductive mechanisms in various RH levels. The initial current always is conveyed by ions and electrons while the final current is only just conveyed by electrons.[48]

When the TiO_2-EA sensor is exposed to a very low RH level (10%), the current is very weak to be nearly a constant current value (Figure 5a). This indicates that only one type of charge carrier dominates the conduction process in 10% RH. Combined with the results of AC impedance spectra measurements, it can be concluded that the charge carrier is the intrinsic electron. Since both the coordinated and free amino groups of TiO_2-EA contain lone electrons, it is more conducive to the migration of free electrons under low humidity conditions. Therefore, the humidity sensing performance of TiO_2-EA is significantly better than that of TiO_2-EG and TiO_2-OA under ultra-low humidity conditions, while the $-COO^-$ of TiO_2-OA is an electron-withdrawing group that is not beneficial for migration of electrons. With the relative humidity growing higher, both the initial and final currents increase (Figure 5b), but former increases more distinctly than the latter, indicating a contribution of ionic conduction and suggesting the ionic current increases more rapidly than the electronic one. Because the ions cannot pass through the electrode, they accumulate on the interface of sensing film/electrodes, thus causing the initial current to decrease more sharply than final current. This phenomenon is also consistent with the diffusion process of H_3O^+ and H^+ in AC impedance plots, and further confirms that the ion conduction is another contribution for conductive mechanism. When the humidity reaches high humidity levels, there is a small raised peak in the total current curve of TiO_2-EA (Figure 5c–5d). This indicates that the ion diffusion conduction becomes the dominant conductive process completely.[49]

n CONCLUSION

In summary, three 2D ultra-thin TiO_2 nanosheet samples with different functional groups were successfully prepared via a solvothermal method and a facile post-ligand modification strategy. The effect of different surface coordination environments for humidity sensing applications was systematically investigated. Due to the superiority in specific surface area (~320 $m^2 \cdot g^{-1}$) and the electron-donating amino groups on TiO_2 surface, the TiO_2-EA sensors exhibit outstanding sensing performance with a short response time (98.4 s), narrow hysteresis, and good fitting linearity (R^2 = 0.994) at the RH range of 10–98%, as well as a limit of detection (15 ppm) for ultra-low humidity sensing. The possible sensing mechanism is hypothesized by AC complex spectrum measurements and DC instantaneous reverse polarity experiments, which reveal the different conduction behaviors at various RH levels. This work not only demonstrates the specific perspective in developing high-performance 2D nanostructured sensing materials via the modulation of surface micro-environment, but also offers a little insight into the application of surface chemistry in the field of IoT and AI.

n ACKNOWLEDGEMENTS

This work is supported by the National Natural Science Foundation of China (21905280, 22171263, 91961115, 22175176 and 21975254), National Natural Science Foundation of Fujian (2021J02017 and 2020J01109) and Youth Innovation Promotion Association CAS.

n AUTHOR INFORMATION

Corresponding authors. Emails: gxu@fjirsm.ac.cn (G. Xu) and yexl@fjirsm.ac.cn (X. Ye)

n COMPETING INTERESTS

The authors declare no competing interests.

n ADDITIONAL INFORMATION

Supplementary information is available for this paper at http://manu30.magtech.com.cn/jghx/EN/10.14102/j.cnki.0254-5861.2022-0046

For submission: https://mc03.manuscriptcentral.com/cjsc

n REFERENCES

(1) Trung, T. Q.; Duy, L. T.; Ramasundaram, S.; Lee, N. E. Transparent, stretchable, and rapid-response humidity sensor for body-attachable wearable electronics. *Nano Res.* **2017**, 10, 2021–2033.

(2) Yao, S.; Myers, A.; Malhotra, A.; Lin, F.; Bozkurt, A.; Muth, J. F.; Zhu, Y. A wearable hydration sensor with conformal nanowire electrodes. *Adv. Healthcare Mater.* **2017**, 6, 1601159.

(3) Wang, X.; Xiong, Z.; Liu, Z.; Zhang, T. Exfoliation at the liquid/air interface to assemble reduced graphene oxide ultrathin films for a flexible noncontact sensing device. *Adv. Mater.* **2015**, 27, 1370–1375.

DOI: 10.14102/j.cnki.0254-5861.2022-0046

(4) Zhao, J.; Li, N.; Yu, H.; Wei, Z.; Liao, M.; Chen, P.; Wang, S.; Shi, D.; Sun, Q.; Zhang, G. Highly sensitive MoS_2 humidity sensors array for noncontact sensation. *Adv. Mater.* **2017**, 29, 1702076.
(5) Cheng, H.; Huang, Y.; Cheng, Q.; Shi, G.; Jiang, L.; Qu, L. Self-healing graphene oxide based functional architectures triggered by moisture. *Adv. Funct. Mater.* **2017**, 27, 1703096.
(6) Botta, A.; de Donato, W.; Persico, V.; Pescape, A. Integration of cloud computing and Internet of things: a survey. *Futur. Gener. Comp. Syst.* **2016**, 56, 684–700.
(7) Zhao, J.; Li, N.; Yu, H.; Wei, Z.; Liao, M.; Chen, P.; Wang, S.; Shi, D.; Sun, Q.; Zhang, G. Highly sensitive MoS_2 humidity sensors array for noncontact sensation. *Adv. Mater.* **2017**, 29, 1702076.
(8) Li, X.; Feng, W. D.; Zhang, X. X.; Wang, W.; Chen, S. J.; Zhang, Y. N. Fabrication of humidity sensors based on laser scribed graphene oxide/SnO_2 composite layers. *Chin. J. Struct. Chem.* **2020**, 39, 1949–1957.
(9) Yang, S. X.; Jiang, C. B.; Wei, S. H. Gas sensing in 2D materials. *Appl. Phys. Rev.* **2017**, 4, 021304.
(10) Zhang, L.; Khan, K.; Zou, J. F.; Zhang, H.; Li, Y. C. Recent advances in emerging 2D material-based gas sensors: potential in disease diagnosis. *Adv. Mater. Interfaces* **2019**, 6, 1901329.
(11) Buckley, D. J.; Black, N. C. G.; Castanon, E. G.; Melios, C.; Hardman, M.; Kazakova, O. Frontiers of graphene and 2D material-based gas sensors for environmental monitoring. *2D Mater.* **2020**, 7, 032002.
(12) Fu, Q.; Bao, X. Surface chemistry and catalysis confined under two-dimensional materials. *Chem. Soc. Rev.* **2017**, 46, 1842–1874.
(13) Ye, X. L.; Lin, S. J.; Zhang, J. W.; Jiang, H. J.; Cao, L. A.; Wen, Y. Y.; Yao, M. S.; Li, W. H.; Wang, G. E.; Xu, G. Boosting room temperature sensing performances by atomically dispersed Pd stabilized via surface coordination. *ACS Sens.* **2021**, 6, 1103–1110.
(14) Ye, X. L.; Gu, Y. G.; Wang, C. M. Fabrication of the Cu_2O/polyvinyl pyrrolidone-graphene modified glassy carbon-rotating disk electrode and its application for sensitive detection of herbicide paraquat. *Sens. Actuators, B* **2012**, 173, 530–539.
(15) Ye, X. L.; Huang, Y. Q.; Tang, X. Y.; Xu, J.; Peng, C.; Tan, Y. Z. Two-dimensional extended π-conjugated triphenylene-core covalent organic polymer. *J. Mater. Chem. A* **2019**, 7, 3066–3071.
(16) Chen, X.; Liu, L.; Huang, F. Black titanium dioxide (TiO_2) nanomaterials. *Chem. Soc. Rev.* **2015**, 44, 1861–1885.
(17) Liu, M.; Chen, Y. J.; Huang, X.; Dong, L. Z.; Lu, M.; Guo, C.; Yuan, D.; Chen, Y.; Xu, G.; Li, S. L.; Lan, Y. Q. Porphyrin-based COF 2D materials: variable modification of sensing performances by post-metallization. *Angew. Chem. Int. Ed.* **2022**, e202115308.
(18) Lu, M.; Zhang, M.; Liu, J.; Chen, Y.; Liao, J. P.; Yang, M. Y.; Cai, Y. P.; Li, S. L.; Lan, Y. Q. Covalent organic framework based functional materials: important catalysts for efficient CO_2 utilization. *Angew. Chem. Int. Ed.* **2022**, e202200003.
(19) Hu, Y. J.; Yin, Y. H.; Zhang, M.; Wu, Z. P.; Shen, Z. R. In-situ growth of carbon nanosheets intercalated with TiO_2 for improving electrochemical performance and stability of lithium-ion batteries. *Chin. J. Struct. Chem.* **2021**, 40, 1513–1524.
(20) Qin, R.; Liu, K.; Wu, Q.; Zheng, N. Surface coordination chemistry of atomically dispersed metal catalysts. *Chem. Rev.* **2020**, 120, 11810–11899.
(21) Liu, P.; Qin, R.; Fu, G.; Zheng, N. Surface coordination chemistry of metal nanomaterials. *J. Am. Chem. Soc.* **2017**, 139, 2122–2131.
(22) Deshmukh, K.; Kovarik, T.; Pasha, S. K. K. State of the art recent progress in two dimensional MXenes based gas sensors and biosensors: a comprehensive review. *Coord. Chem. Rev.* **2020**, 424, 213514.
(23) Zhao, C. J.; Wu, H. R. A first-principles study on the interaction of biogas with noble metal (Rh, Pt, Pd) decorated nitrogen doped graphene as a gas sensor: a DFT study. *Appl. Surf. Sci.* **2018**, 435, 1199–1212.
(24) Pan, L.; Liu, Y. T.; Zhong, M.; Xie, X. M. Coordination-driven hierarchical assembly of hybrid nanostructures based on 2D materials. *Small* **2020**, 16, 1902779.
(25) Meng, Z.; Stolz, R. M.; Mendecki, L.; Mirica, K. A. Electrically-transduced chemical sensors based on two-dimensional nano-materials. *Chem. Rev.* **2019**, 119, 478–598.
(26) Wang, S.; Wang, R.; Wang, X.; Zhang, D.; Qiu, X. Nanoscale charge distribution and energy band modification in defect-patterned graphene. *Nanoscale* **2012**, 4, 2651–2657.
(27) Guo, Y.; Xu, K.; Wu, C.; Zhao, J.; Xie, Y. Surface chemical-modification for engineering the intrinsic physical properties of inorganic two-dimensional nanomaterials. *Chem. Soc. Rev.* **2015**, 44, 637–646.
(28) Liu, J.; Tang, J.; Gooding, J. J. Strategies for chemical modification of graphene and applications of chemically modified graphene. *J. Mater. Chem.* **2012**, 22, 12435–12452.
(29) Choi, S. J.; Jang, J. S.; Park, H. J.; Kim, I. D. Optically sintered 2D RuO_2 nanosheets: temperature-controlled NO_2 reaction. *Adv. Funct. Mater.* **2017**, 27, 1606026.
(30) ten Elshof, J. E.; Yuan, H.; Gonzalez Rodriguez, P. Two-dimensional metal oxide and metal hydroxide nanosheets: synthesis, controlled assembly and applications in energy conversion and storage. *Adv. Energy Mater.* **2016**, 6, 1600355.
(31) Miao, J.; Chen, C.; Meng, L.; Lin, Y. Self-assembled monolayer of metal oxide nanosheet and structure and gas-sensing property relationship. *ACS Sens.* **2019**, 4, 1279–1290.
(32) Pawar, M. S.; Bankar, P. K.; More, M. A.; Late, D. J. Ultra-thin V_2O_5 nanosheet based humidity sensor, photodetector and its enhanced field emission properties. *RSC Adv.* **2015**, 5, 88796–88804.
(33) Szendrei, K.; Ganter, P.; Sànchez-Sobrado, O.; Eger, R.; Kuhn, A.; Lotsch, B. V. Touchless optical finger motion tracking based on 2D nanosheets with giant moisture responsiveness. *Adv. Mater.* **2015**, 27, 6341–6348.
(34) Zhang, P.; Zhang, L. X.; Xu, H.; Xing, Y.; Chen, J. J.; Bie, L. J. Ultrathin CeO_2 nanosheets as bifunctional sensing materials for humidity and formaldehyde detection. *Rare Metals* **2021**, 40, 1614–1621.
(35) Choi, S. J.; Kim, I. D.; Park, H. J. 2D layered Mn and Ru oxide nanosheets for real-time breath humidity monitoring. *Appl. Surf. Sci.* **2022**, 573, 151481.
(36) Tsai, F. S.; Wang, S. J. Enhanced sensing performance of relative humidity sensors using laterally grown ZnO nanosheets. *Sens. Actuators, B* **2014**, 193, 280–287.

DOI: 10.14102/j.cnki.0254-5861.2022-0046

(37) Gong, M.; Li, Y.; Guo, Y.; Lv, X.; Dou, X. 2D TiO_2 nanosheets for ultrasensitive humidity sensing application benefited by abundant surface oxygen vacancy defects. *Sens. Actuators, B* **2018**, 262, 350–358.
(38) Marchand, R.; Brohan, L.; Tournoux, M. TiO_2(B) a new form of titanium-dioxide and the potassium octatitanate $K_2Ti_8O_{17}$. *Mater. Res. Bull.* **1980**, 15, 1129–1133.
(39) Liu, P.; Zhao, Y.; Qin, R.; Mo, S.; Chen, G.; Gu, L.; Chevrier, D. M.; Zhang, P.; Guo, Q.; Zang, D.; Wu, B.; Fu, G.; Zheng, N. Photochemical route for synthesizing atomically dispersed palladium catalysts. *Science* **2016**, 352, 797–801.
(40) Guo, W.; Zou, J. H.; Guo, B. B.; Xiong, J. H.; Liu, C.; Xie, Z. H.; Wu, L. Pd nanoclusters/TiO_2(B) nanosheets with surface defects toward rapid photocatalytic dehalogenation of polyhalogenated biphenyls under visible light. *Appl. Catal., B* **2020**, 277.
(41) Xiong, J.; Wen, L.; Jiang, F.; Liu, Y.; Liang, S.; Wu, L. Ultrathin HNb_3O_8 nanosheet: an efficient photocatalyst for the hydrogen production. *J. Mater. Chem. A* **2015**, 3, 20627–20632.
(42) Kapica-Kozar, J.; Pirog, E.; Kusiak-Nejman, E.; Wrobel, R. J.; Gesikiewicz-Puchalska, A.; Morawski, A. W.; Narkiewicz, U.; Michalkiewicz, B. Titanium dioxide modified with various amines used as sorbents of carbon dioxide. *New J. Chem.* **2017**, 41, 1549–1557.
(43) Nakayama, N.; Hayashi, T. Preparation of TiO_2 nanoparticles surface-modified by both carboxylic acid and amine: dispersibility and stabilization in organic solvents. *Colloids Surf., A* **2008**, 317, 543–550.
(44) Chen, Z.; Sun, Y.; Zhang, W.; Yang, T.; Chen, L.; Yang, R.; Zhou, N. Controllable synthesis of amine-functionalized Fe_3O_4 polyhedra for lipase immobilization. *CrystEngComm* **2016**, 18, 3124–3129.
(45) Bhati, V. S.; Kumar, M.; Banerjee, R. Gas sensing performance of 2D nanomaterials/metal oxide nanocomposites: a review. *J. Mater. Chem. C* **2021**, 9, 8776–8808.
(46) Li, J.; Fu, T.; Chen, Y.; Guan, B.; Zhuo, M.; Yang, T.; Xu, Z.; Li, Q.; Zhang, M. Highly sensitive humidity sensors based on Sb-doped $ZnSnO_3$ nanoparticles with very small sizes. *CrystEngComm* **2014**, 16, 2977–2983.
(47) Wang, C. P.; Kashi, C.; Ye, X. L.; Li, W. H.; Wang, G. E.; Xu, G. A zinc based coordination polymer: multi-functional material for humidity sensor and fluorescence applications. *Chin. J. Struct. Chem.* **2021**, 40, 1138–1144.
(48) Li, H.; Fan, H.; Liu, Z.; Zhang, J.; Wen, Y.; Lu, J.; Jiang, X.; Chen, G. Highly sensitive humidity sensor based on lithium stabilized Na-β"-alumina: dc and ac analysis. *Sens. Actuators, B* **2018**, 255, 1445–1454.
(49) Wang, R.; He, Y.; Zhang, T.; Wang, Z.; Zheng, X.; Niu, L.; Wu, F. DC and AC analysis of humidity sensitive properties based on K^+ doped nanocrystalline $LaCo_{0.3}Fe_{0.7}O_3$. *Sens. Actuators, B* **2009**, 136, 536–540.

Received: March 4, 2022
Accepted: March 29, 2022
Published: April 8, 2022

DOI: 10.14102/j.cnki.0254-5861.2022-0046